

Nonergodicity of confined superdiffusive fractional Brownian motion

Yingjie Liang^{1,2,*}, Wei Wang^{1,2,†}, Ralf Metzler^{2,3,‡} and Andrey G. Cherstvy^{2,§}

¹College of Mechanics and Materials, Hohai University, 211100 Nanjing, China

²Institute of Physics and Astronomy, University of Potsdam, 14476 Potsdam, Germany

³Asia Pacific Center for Theoretical Physics, Pohang 37673, Republic of Korea



(Received 28 July 2023; accepted 3 October 2023; published 1 November 2023)

Using stochastic simulations supported by analytics we determine the degree of nonergodicity of box-confined fractional Brownian motion for both sub- and superdiffusive Hurst exponents H . At $H > 1/2$ the nonequivalence of the ensemble- and time-averaged mean-squared displacements (TAMSDs) is found to be most pronounced (with a giant spread of individual TAMSDs at $H \rightarrow 1$), with two distinct short-lag-time TAMSD exponents.

DOI: [10.1103/PhysRevE.108.L052101](https://doi.org/10.1103/PhysRevE.108.L052101)

Introduction. Fractional Brownian motion (FBM) in free space [1,2] is a non-Markovian nonaging stochastic process with a Gaussian probability-density function (PDF) $p(x, t)$ of particle displacements x at time t . For one-dimensional FBM, both the ensemble-averaged mean-squared displacement (MSD) $\langle x^2(t) \rangle = \int_{-\infty}^{+\infty} x^2 p(x, t) dx$ and the mean over N traces $\overline{\langle \delta^2(\Delta) \rangle} = N^{-1} \sum_{i=1}^N \overline{\delta_i^2(\Delta)}$ of the time-averaged MSDs (TAMSDs) $\overline{\delta_i^2(\Delta)} = \frac{1}{T-\Delta} \int_0^{T-\Delta} [x_i(t+\Delta) - x_i(t)]^2 dt$ grow nonlinearly. Here, T is the total time and Δ is the time lag. FBM at $\Delta \ll T$ is ergodic [3–6] in the sense of Boltzmann-Birkhoff-Khinchin [7], i.e.

$$\langle x^2(\Delta) \rangle \approx \overline{\langle \delta^2(\Delta) \rangle} \approx 2K_{2H} \Delta^{2H}, \quad (1)$$

where K_{2H} is the generalized diffusion coefficient and H is the Hurst exponent [8]. The overline denotes averaging over time, and the angular brackets stand for ensemble averaging [7]. FBM rationalizes, *inter alia*, subdiffusive motion of components and tracers in biological cells [6,7,9].

Statistical properties of box-confined [10–19] or reset [20,21] FBM are more intricate. Subdiffusive confined FBM initially grows as [11] (1) and reaches H -dependent stationary (st) plateaus at long [16] times (Fig. 1),

$$\text{MSD}_{\text{st}} \approx \text{TAMSD}_{\text{st}}/2 \approx [3H/(2-H)] \times L^2/12. \quad (2)$$

From the MSD and PDF perspective, FBM near a boundary and confined in potentials [22] was studied. Superdiffusive confined FBM was, however, not examined from a TAMSD viewpoint: its behavior offers surprises (see below). We bridge this gap here, also complementing the TAMSD results [10,11] for confined FBM at $H < 1/2$.

Main equations. Free FBM is formulated via the overdamped (high-viscosity limit) stochastic differential equation $dx(t)/dt = \eta_H(t)$ driven by external fractional Gaussian

noise $\eta_H(t)$ with correlations

$$\langle \eta_H(t_1) \eta_H(t_2) \rangle \approx 2K_{2H} H(2H-1) \times |t_1 - t_2|^{2H-2}. \quad (3)$$

Brownian motion (BM) follows from FBM at $H = 1/2$, superdiffusive FBM at $1/2 < H < 1$ features positive correlations, while subdiffusive FBM at $0 < H < 1/2$ has negative correlations [7]. Nonthermalized nonequilibrium FBM [2] differs from conventional BM driven by a memoryless white noise and satisfying the fluctuation-dissipation relation.

FBM in a box $x \in [-L/2, L/2]$ —discretized at times $t_j = j \times dt$ with the time step $dt = \Delta_1 = T/\bar{N}$ (\bar{N} is the number of points)—obeys the recursive relation

$$x(t_{j+1}) = \begin{cases} x(t_j) + dB_H(t_j), & |x(t_j) + dB_H(t_j)| \leq L/2 \\ x(t_j), & \text{otherwise.} \end{cases} \quad (4)$$

The increments $dB_H(t_n) = \eta_H(t_n)dt$ are Gaussian and have zero mean $\langle dB_H \rangle = 0$, second moment $\langle dB_H^2 \rangle = 2K_{2H}(dt)^{2H}$, and covariance function $\langle dB_H(t_m) dB_H(t_{m+j}) \rangle = 2K_{2H}(dt)^{2H} (|j+1|^{2H} - 2|j|^{2H} + |j-1|^{2H})$. Using the free-FBM code [4,6], we simulate confined FBM with “inelastic” reflections, (4) (Fig. 4). Other schemes [13] yield similar results if the one-step-MSD satisfies $L_1^2 = 2K_{2H}(dt)^{2H} \ll L^2$.

Results. Due to persistence of consecutive jumps, superdiffusive FBM after a reflection (4) hits the boundary repeatedly. The opposite is true for subdiffusive FBM (Fig. 4). Thus, at $H > 1/2$ FBM particles accumulate and at $H < 1/2$ they deplete near a boundary [12,14,16,23] (Fig. 5). This effect persists for other reflection schemes and for massive FBM [5] in a box (not shown). A power-law PDF quantifying these features is [12,14], $p_1(x) \propto |x - L/2|^{1/H-2}$. A stationary “symmetric” PDF valid in the entire x interval (Fig. 5) is [24,25]

$$p_{2,\text{st}}(x) \approx C_H L^{-1} [(-x/L + 1/2)(x/L + 1/2)]^{1/H-2}, \quad (5)$$

where $C_H = \Gamma(1/H - 1/2)/[2^{3-2/H} \sqrt{\pi} \Gamma(1/H - 1)]$ and $\Gamma(z)$ is the Gamma function. The PDF (5) yields the MSD_{st} (2) (Fig. 6), while $\text{MSD}_{\text{st}} = L^2/4$ at $H \rightarrow 1$ (ballistic motion). In contrast, the PDF of box-confined BM is uniform, $p_{\text{st}}(x) = 1/L$, yielding [16] $\text{MSD}_{\text{st}} = L^2/12$.

*liangyj@hhu.edu.cn

†weiwanguaa@gmail.com

‡rmetzler@uni-potsdam.de

§a.cherstvy@gmail.com

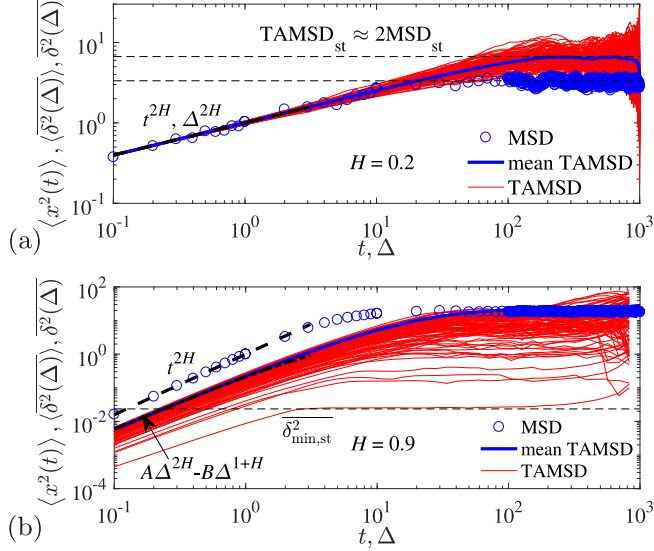


FIG. 1. MSD, mean TAMSD, and sample realizations of the TAMSDs of confined FBM for the (a) subdiffusive ($H = 0.2$) and (b) superdiffusive ($H = 0.9$) case. The free-FBM MSDs (1) are the dashed lines; the dot-dashed curve for $\langle \delta^2(\Delta) \rangle$ is Eq. (7), with its scaling behaviors indicated. The levels $\text{MSD}_{\text{st}} \approx \text{TAMSD}_{\text{st}}/2$ and the plateau $\delta_{\text{min,st}}^2$ are shown in panels (a) and (b), respectively. At the last point, $\text{MSD}(T) = \langle \text{TAMSD}(T) \rangle$. Parameters: the trajectory length is $T = 10^3$, the simulation step is $dt = 10^{-1}$, the diffusion coefficient is $K_{2H} = 1/2$, the number of trajectories is $N = 300$, the number of points is $\bar{N} = 10^4$, and the box size is $L = 10$.

The MSD and mean TAMSD of *subdiffusive* confined FBM behave—at chosen values of T , L , and dt —as expected [10,11] (Fig. 1). Namely, after an H -dependent short-time nearly unperturbed growth (1), a plateau of the MSD (attained in a power-law manner [11]) and a twice-as-high TAMSD_{st} (2) are reached at long times after multiple reflections [Fig. 1(a)].

Surprisingly, for $H > 1/2$ and at short (lag) times neither the scalings nor the magnitudes of the MSD and TAMSD match (nonergodicity [7]). The TAMSD reaches the plateau at later times than the MSD, due to a slower TAMSD(Δ) growth [see Eq. (7)]. Depending on the values of $H > 1/2$ and T , the TAMSD might not yet be stationary, whereas the MSD_{st} is already attained (not shown). At $H > 1/2$, due to a scatter of the TAMSD plateaus, each $\delta_i^2(\Delta)$ contributes differently to the evolution of $\langle \delta^2(\Delta) \rangle$.

The lowest TAMSD plateau $\delta_{\text{min,st}}^2$ can be assessed as follows. For $H \rightarrow 1$ the process at $\Delta = \Delta_{\text{st}}$ ballistically reaches $x = \pm L/2$ with a velocity such that $v\Delta_{\text{st}} \sim L/2$ and continues “hitting” the boundary after that. For such traces, for $\Delta \gg \Delta_{\text{st}}$ the increments in the TAMSD are $[x(t + \Delta) - x(t)]^2 \sim (L/2 - vt)^2$, yielding the plateau $\delta_{\text{min,st}}^2 \sim (\Delta_{\text{st}}/T) \times (L^2/12)$ [see Fig. 1(b)]. Multiple higher $\delta_{\text{st},i}^2$ plateaus found in this plot are due to more than one reflection.

Analytically, for the i th trace of confined FBM (4), n_i reflections occur at times $\{t_{\text{refl},i,1}, t_{\text{refl},i,2}, \dots, t_{\text{refl},i,n_i}\}$. All \bar{N} steps can thus be divided into a set of reflective and diffusive $\{t_{\text{diff},i,1}, t_{\text{diff},i,2}, \dots, t_{\text{diff},i,\bar{N}-n_i}\}$ steps. As per Eq. (4), the increments for diffusive steps are $x(t_{\text{diff},i,k} + dt) -$

$x(t_{\text{diff},i,k}) = dB_H(t_{\text{diff},i,k})$, while at reflection events $x(t_{\text{refl},i,k} + dt) - x(t_{\text{refl},i,k}) = 0$. At the shortest lag time $\Delta_1 = dt$ we get $\delta_i^2(\Delta_1) = \frac{\Delta_1}{T - \Delta_1} \sum_{j=1}^{\bar{N}} \{x_i[(j+1)dt] - x_i(jdt)\}^2$ that gives $\overline{\delta_i^2(\Delta_1)} = \frac{1}{\bar{N}-1} \sum_{k=1}^{\bar{N}-n_i} dB_H^2(t_{\text{diff},i,k})$. After ensemble averaging at $\bar{N} \gg 1$ with $\langle dB_H^2 \rangle$ one gets $\overline{\langle \delta^2(\Delta_1) \rangle} \approx 2K_{2H}(1 - \langle n \rangle / \bar{N}) \Delta_1^{2H}$, with $\langle n \rangle = N^{-1} \sum_{i=1}^N n_i$. Thus, the difference $\text{MSD}(\Delta_1) - \text{TAMSD}(\Delta_1)$ related to nonergodicity is expressed via a reflection “rate,” $\langle n \rangle / \bar{N}$. The PDF (5) at $L_1 \ll L$ gives $\langle n \rangle / \bar{N} = 2 \int_{L/2-L_1}^{L/2} p_{2,\text{st}}(x) dx \approx D_H (L_1/L)^{1/H-1}$, where $D_H = 2C_H / (1/H - 1)$. This yields a fraction of time steps a particle, located within L_1 from a boundary, is reflected within time dt . At $H = 1/2$ this yields $\langle n \rangle / \bar{N} = 2L_1/L$ [uniform $p_{\text{st}}(x)$]. Using L_1 with $dt = \Delta_1$ we get

$$\langle n \rangle / \bar{N} \approx D_H (\sqrt{2K_{2H}})^{1/H-1} (T/\bar{N})^{1-H} L^{1-1/H}, \quad (6)$$

in agreement with the *in silico* results for varying L and \bar{N} (Fig. 7) [the same scalings follow from $p_1(x)$]. From $\langle \delta^2(\Delta_1) \rangle$ with Eq. (6) the short-lag-time TAMSD is

$$\overline{\langle \delta^2(\Delta) \rangle} \approx 2K_{2H} \Delta^{2H} - D_H (2K_{2H})^{\frac{1/H+1}{2}} L^{1-1/H} \Delta^{1+H}. \quad (7)$$

At short Δ the first term in Eq. (7) dominates ($\propto \Delta^{2H}$ prior to a first reflection), especially for $H < 1/2$. Thus, $\text{MSD}(\Delta_1) - \text{TAMSD}(\Delta_1)$ is small for subdiffusive confined FBM (as studied in Refs. [10,11], where the effect was missed); it is significant for $H > 1/2$ (and especially for $H \rightarrow 1$). A L - and T -dependent second term in Eq. (7) at intermediate Δ [Fig. 1(b)] has $\propto \Delta^{1+H}$ scaling. Its magnitude agrees with simulations (Fig. 8). For $H < 1/2$ the reflection rate decays quicker with T and L than for $H > 1/2$ (Fig. 7). Thus, for realistic L the $\langle n \rangle / \bar{N}$ is much smaller than for superdiffusive FBM [the term $\propto \Delta^{1+H}$ in (7) is most relevant].

Two distinct TAMSD exponents and $\text{MSD}(\Delta_1) \neq \text{TAMSD}(\Delta_1)$ were also detected for reset FBM [20,21] at $H > 1/2$ [see Eq. (44) in Ref. [21]]. Ergodicity (1) was, however, restored for the increment-MSD (iMSD) [21], i.e., $\text{iMSD}(\Delta) = \text{TAMSD}(\Delta)$. The same is true for confined FBM at $H > 1/2$, both for small and large Δ values (not shown), with the iMSD computed at [21] $\Delta \gg \Delta_{\text{st}}$. A pronounced $\overline{\delta_i^2(\Delta_1)}$ spread and large $\text{EB}(\Delta_1)$ values render $H > 1/2$ FBM under reset and in a box *still nonergodic* in the sense that $\text{EB} \gg \text{EB}_{\text{BM}}$. Other confined processes treated as nonergodic might feature $\text{iMSD} = \text{TAMSD}$.

The $\overline{\delta_i^2(\Delta)}$ spread—described by the PDF [7] $\phi(\xi)$ with $\xi(\Delta) = \delta^2(\Delta) / \overline{\delta^2(\Delta)}$ —is small for sub- and substantial for superdiffusive confined FBM (Fig. 2). For the latter, the $\phi(\xi)$ -PDF is profoundly skewed (as larger increments dx are prohibited by reflections from the box boundaries), leading to smaller TAMSD entries. The scatter is quantified by the ergodicity-breaking parameter [7] EB —the squared coefficient of variation or squared relative standard deviation of the $\overline{\delta_i^2(\Delta)}$ distribution— $\text{EB}(\Delta) = \langle \xi^2(\Delta) \rangle - 1$. The values of $\text{EB}(\Delta_1)$ for box-confined FBM at $H < 1/2$ are small, in contrast to $\text{EB}(\Delta_1)$ at $H > 1/2$ (Fig. 3). Concretely, at $\Delta = \Delta_1$ the EB at $H \rightarrow 1$ is $\sim 10^3$ that of confined BM (Fig. 3).

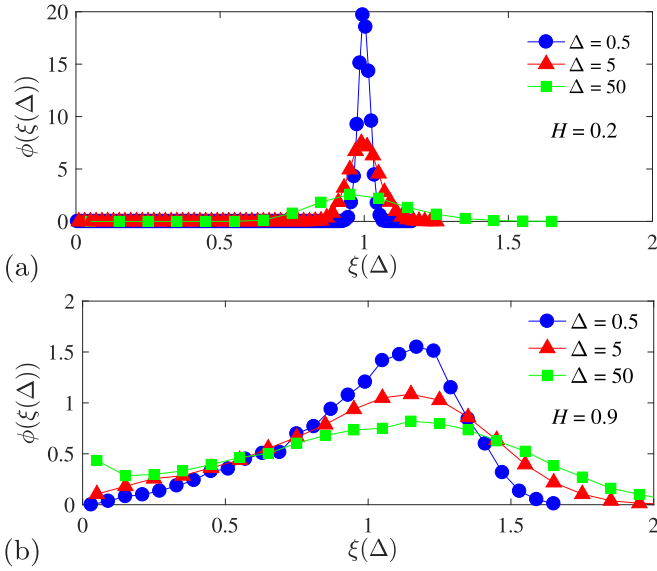


FIG. 2. PDF of the TAMSD distribution $\phi(\xi(\Delta))$ computed from Fig. 1 for the same parameters, at several Δ values.

We compare $EB(\Delta)$ -vs- H behavior in Figs. 3 and 9 to that of free FBM [3], also growing at $H > 1/2$ and thus indicating nonergodicity. For free FBM, we have [3,4] $EB_{H < 3/4}(\Delta/T) \sim (\Delta/T)^1$ and $EB_{H > 3/4}(\Delta/T) \sim (\Delta/T)^{4-4H}$. For confined FBM, the simulations still show $EB_{H < 1/2}(\Delta/T) \sim (\Delta/T)^1$, while we get $EB_{H > 1/2}(\Delta/T) \sim (\Delta/T)^{2-2H}$ (Fig. 9). The latter scaling follows by replacing $2H$ in $(4 - 2 \times 2H)$ with the new TAMSD exponent $(H + 1)$ [Eq. (7)]. The border of the EB-scaling regimes thus shifts from the free FBM's [3] $H = 3/4$ to $1/2$ for FBM in a box. Intuitively, for confined subdiffusive FBM—only slightly affected by reflections—the linear EB(Δ/T) law stays unaltered, while for superdiffusive FBM in a box the scaling of EB changes (for $H > 1/2$ and not for $H > 3/4$). The above EB(Δ/T)-dependencies feature continuous exponents at these critical H values. Inertia also triggers nonergodicity of free “massive” FBM [5].

Discussion. Box-confined FBM is generally nonergodic in the sense of (1). While its ergodicity is often true for $H < 1/2$, it fails drastically for $H > 1/2$ where

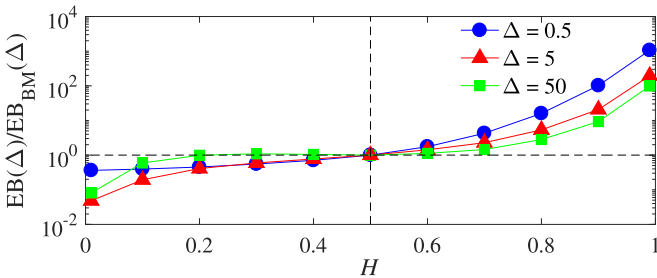


FIG. 3. EB parameter of confined FBM computed from Fig. 2 and normalized to EB of box-confined BM, $EB_{BM}(\Delta)$.

$MSD(\Delta_1) \neq TAMSD(\Delta_1)$ and the scatter of $\overline{\delta_i^2(\Delta_1)}$ is not sharp. Implications of these results for FBM-based description of—particularly superdiffusive—time series in single-particle-tracking experiments can be farreaching. For instance, the distribution of serotonergic fibers in the brain with reflecting boundaries was modeled as superdiffusive confined FBM [26,27]. For other *in vitro* and *in silico* datasets of FBM type these nonergodicity aspects are to be checked in the future.

Acknowledgments. Y.L. and R.M. acknowledge financial support from, respectively, the Alexander von Humboldt Foundation (Grant No. 1217531) and the German Science Foundation (DFG Grant No. ME 1535/12-1).

Appendix: In Figs. 4–9 we present supplementary plots.

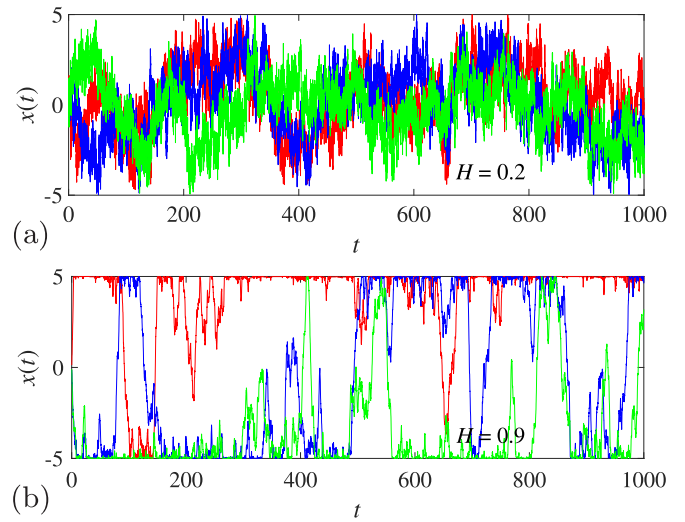


FIG. 4. Exemplary traces of confined FBM for (a) subdiffusive and (b) superdiffusive H values.

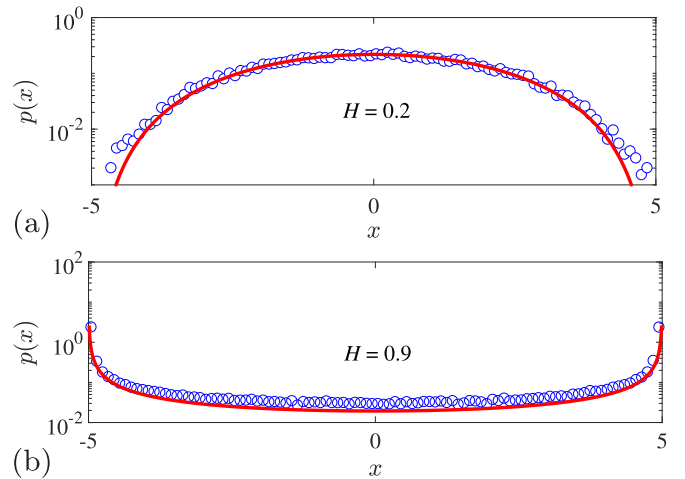


FIG. 5. PDFs of sub- and superdiffusive box-confined FBM. The solid curves are given by Eq. (5).

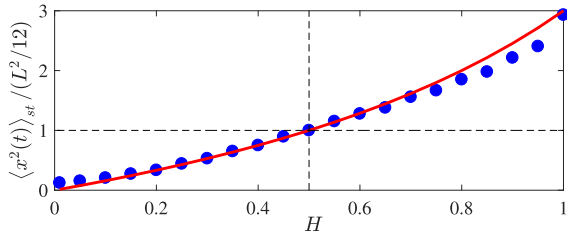


FIG. 6. Stationary MSD plateaus normalized to MSD_{st} of BM: Eq. (2) is shown vs the simulation results (dots). Note some slight deviations for very superdiffusive FBM.

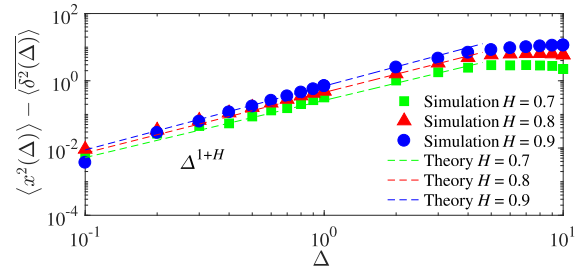


FIG. 8. Short-time $[\text{MSD}(\Delta) - \text{TAMSD}(\Delta)]$ deviations at $H > 1/2$, compared to Eq. (7). Parameters: $T = 10^3, L = 10$.

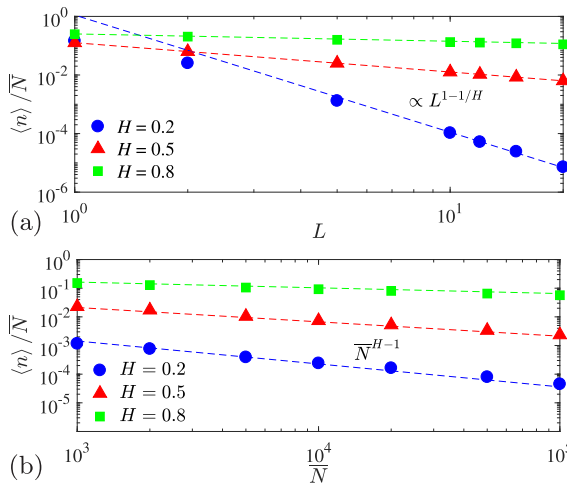


FIG. 7. Reflection rate for box-confined FBM. Scaling dependencies by Eq. (6) with parameters (a) L ($\bar{N} = 10^6, dt = 0.1$) and (b) \bar{N} ($L = 10, T = 10^2$) are the dashed lines.

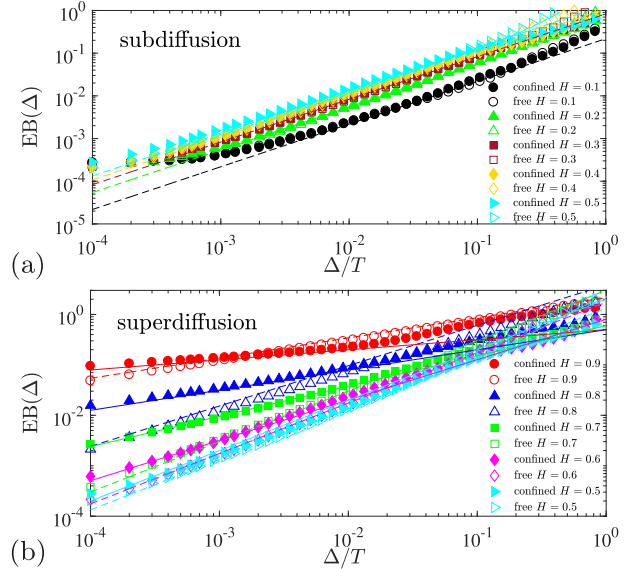


FIG. 9. EB variation for (a) subdiffusive and (b) superdiffusive free and confined FBM (empty and filled symbols, respectively). Linear scalings $\text{EB}_{H < 1/2}(\Delta/T)$ in (a) are the dashed lines. Relations $\text{EB}_{H > 3/4}(\Delta/T)$ for free FBM [3] and $\text{EB}_{H > 1/2}(\Delta/T)$ for confined FBM in (b) are the dashed and continuous lines, respectively. We observe quantifiable [4] time-step-discreteness-induced deviations at short Δ in (a) and some long-lag-time deviations of EB from the asymptotes because of deterioration of TAMSD-averaging statistics.

[1] A. N. Kolmogorov, Dokl. Akad. Nauk. SSSR [Sov. Phys. Dokl.] **26**, 115 (1940).
 [2] B. B. Mandelbrot and J. W. van Ness, *SIAM Rev.* **10**, 422 (1968).
 [3] W. Deng and E. Barkai, *Phys. Rev. E* **79**, 011112 (2009).
 [4] W. Wang, A. G. Cherstvy, A. V. Chechkin, S. Thapa, F. Seno, X. Liu, and R. Metzler, *J. Phys. A* **53**, 474001 (2020).
 [5] A. G. Cherstvy, W. Wang, R. Metzler, and I. M. Sokolov, *Phys. Rev. E* **104**, 024115 (2021).
 [6] W. Wang, R. Metzler, and A. G. Cherstvy, *Phys. Chem. Chem. Phys.* **24**, 18482 (2022).
 [7] R. Metzler, J.-H. Jeon, A. G. Cherstvy, and E. Barkai, *Phys. Chem. Chem. Phys.* **16**, 24128 (2014).

[8] H. E. Hurst, *Trans. Am. Soc. Civ. Eng.* **116**, 770 (1951).
 [9] A. Sabri, X. Xu, D. Krapf, and M. Weiss, *Phys. Rev. Lett.* **125**, 058101 (2020).
 [10] J.-H. Jeon and R. Metzler, *Phys. Rev. E* **81**, 021103 (2010).
 [11] J.-H. Jeon and R. Metzler, *Phys. Rev. E* **85**, 021147 (2012).
 [12] A. H. O. Wada and T. Vojta, *Phys. Rev. E* **97**, 020102(R) (2018).
 [13] T. Vojta, S. Skinner, and R. Metzler, *Phys. Rev. E* **100**, 042142 (2019).
 [14] A. H. O. Wada, A. Warhover, and T. Vojta, *J. Stat. Mech.* (2019) 033209.
 [15] A. Malsagov and M. Mandjes, *Phys. Rev. E* **100**, 032120 (2019).
 [16] T. Guggenberger, G. Pagnini, T. Vojta, and R. Metzler, *New J. Phys.* **21**, 022002 (2019).

- [17] T. Vojta, S. Halladay, S. Skinner, S. Januŝonis, T. Guggenberger, and R. Metzler, *Phys. Rev. E* **102**, 032108 (2020).
- [18] T. Vojta and A. Warhover, *J. Stat. Mech.* (2021) 033215.
- [19] T. Vojta, Z. Miller, and S. Halladay, *Eur. Phys. J. B* **94**, 208 (2021).
- [20] W. Wang, A. G. Cherstvy, H. Kantz, R. Metzler, and I. M. Sokolov, *Phys. Rev. E* **104**, 024105 (2021).
- [21] W. Wang, A. G. Cherstvy, R. Metzler, and I. M. Sokolov, *Phys. Rev. Res.* **4**, 013161 (2022).
- [22] T. Guggenberger, A. V. Chechkin, and R. Metzler, *J. Phys. A* **54**, 29LT01 (2021).
- [23] W. R. Holmes, *Biophys. J.* **116**, 1538 (2019).
- [24] K. J. Wiese, *Phys. Rev. E* **99**, 032106 (2019).
- [25] S. N. Majumdar, A. Rosso, and A. Zoia, *Phys. Rev. Lett.* **104**, 020602 (2010).
- [26] S. Januŝonis, K. C. Mays, and M. T. Hingorani, *ACS Chem. Neurosci.* **10**, 3064 (2019).
- [27] S. Januŝonis, N. Detering, R. Metzler, and T. Vojta, *Front. Comput. Neurosci.* **14**, 56 (2020).